Monthly Notices
of the
ROYAL ASTRONOMICAL SOCIETY

Mon. Not. R. Astron. Soc. **411,** 2792–2803 (2011) doi:10.1111/j.1365-2966.2010.17879.x

Discovery of the nearby long, soft GRB 100316D with an associated supernova

R. L. C. Starling,[1⋆] K. Wiersema,[1] A. J. Levan,[2] T. Sakamoto,[3,4,5] D. Bersier,[6] P. Goldoni,[7,8] S. R. Oates,[9] A. Rowlinson,[1] S. Campana,[10] J. Sollerman,[11,12] N. R. Tanvir,[1] D. Malesani,[12] J. P. U. Fynbo,[12] S. Covino,[10] P. D'Avanzo,[10] P. T. O'Brien,[1] K. L. Page,[1] J. P. Osborne,[1] S. D. Vergani,[13,14] S. Barthelmy,[15] D. N. Burrows,[16] Z. Cano,[6] P. A. Curran,[9] M. De Pasquale,[9] V. D'Elia,[17,18] P. A. Evans,[1] H. Flores,[14] A. S. Fruchter,[15] P. Garnavich,[19] N. Gehrels,[4] J. Gorosabel,[20] J. Hjorth,[12] S. T. Holland,[3,4,21] A. J. van der Horst,[22]† C. P. Hurkett,[1] P. Jakobsson,[23] A. P. Kamble,[24] C. Kouveliotou,[22] N. P. M. Kuin,[9] L. Kaper,[24,25] P. A. Mazzali,[26,27,28] P. E. Nugent,[29] E. Pian,[27,30] M. Stamatikos,[4,31]‡ C. C. Thöne[10] and S. E. Woosley[32]

[1]*Department of Physics and Astronomy, University of Leicester, University Road, Leicester LE1 7RH*
[2]*Department of Physics, University of Warwick, Coventry CV4 7AL*
[3]*Center for Research and Exploration in Space Science and Technology (CRESST)*
[4]*NASA Goddard Space Flight Center, Greenbelt, MD 20771, USA*
[5]*Joint Center for Astrophysics, University of Maryland, Baltimore County, 1000 Hilltop Circle, Baltimore, MD 21250, USA*
[6]*Astrophysics Research Institute, Liverpool John Moores University, Birkenhead CH41 1LD*
[7]*Laboratoire Astroparticule et Cosmologie, 10 rue A. Domon et L. Duquet, F-75205 Paris Cedex 13, France*
[8]*DSM/IRFU/Service D'Astrophysique, CEA-Saclay, 91191 Gif-sur-Yvette, France*
[9]*Mullard Space Science Laboratory, University College London, Holmbury St Mary, Dorking, Surrey RH5 6NT*
[10]*INAF-Osservatorio Astronomico di Brera, Via Bianchi 46, I-23807 Merate (LC), Italy*
[11]*The Oskar Klein Centre, Department of Astronomy, Albanova, Stockholm University, SE-106 91 Stockholm, Sweden*
[12]*Dark Cosmology Centre, Niels Bohr Institute, Copenhagen University, Juliane Maries Vej 30, 2100 Copenhagen Ø, Denmark*
[13]*University Paris 7, APC, UMR7164 CNRS, 10 rue Alice Domon et Léonie Duquet, 75205 Paris Cedex 13, France*
[14]*GEPI, Observatoire de Paris, CNRS-UMR 8111, 5 place Jules Janssen, 92195 Meudon, France*
[15]*Space Telescope Science Institute, 3700 San Martin Drive, Baltimore, MD 21218, USA*
[16]*Department of Astronomy and Astrophysics, Pennsylvania State University, 525 Davey Lab, University Park, PA 16802, USA*
[17]*INAF-Osservatorio Astronomico di Roma, Via Frascati 33, I-00040 Monteporzio Catone, Italy*
[18]*ASI-Science Data Centre, Via Galileo Galilei, I-00044 Frascati, Italy*
[19]*Physics Department, University of Notre Dame, Notre Dame, IN 46556, USA*
[20]*Instituto de Astrofísica de Andalucía (IAA-CSIC), Glorieta de la Astronomía s/n, E-18.008 Granada, Spain*
[21]*Universities Space Research Association, 10211 Wincopin Circle, Suite 500, Columbia, MD 21044-3432, USA*
[22]*NASA/Marshall Space Flight Center, Huntsville, AL 35812, USA*
[23]*Centre for Astrophysics and Cosmology, Science Institute, University of Iceland, Dunhagi 5, IS-107 Reykjavik, Iceland*
[24]*Sterrenkundig Instituut Anton Pannekoek, University of Amsterdam, PO number 94249, 1090 GE Amsterdam, the Netherlands*
[25]*Laser Centre, VU University, De Boelelaan 1081, 1081 HV Amsterdam, the Netherlands*
[26]*Max-Planck-Institut für Astrophysik, Karl-Schwarzschild-Strasse 1, 85741 Garching, Germany*
[27]*Scuola Normale Superiore, Piazza Cavalieri 7, 56127 Pisa, Italy*
[28]*INAF Oss. Astron. Padova, vicolo dell'Osservatorio 5, 35122 Padova, Italy*
[29]*Computational Cosmology Center, Lawrence Berkeley National Laboratory, 1 Cyclotron Road, Berkeley, CA 94720, USA*
[30]*Osservatorio Astronomico Di Trieste, Via G. B. Tiepolo, I-34143 Trieste, Italy*
[31]*Department of Physics, The Ohio State University, 191 West Woodruff Avenue, Columbus, OH 43210, USA*
[32]*UCO/Lick Observatory, Department of Astronomy & Astrophysics, University of California, Santa Cruz, CA 95064, USA*

Accepted 2010 October 17. Received 2010 August 19; in original form 2010 April 19

⋆E-mail: rlcs1@star.le.ac.uk
†NASA Postdoctoral Program Fellow.
‡Center for Cosmology and Astro-Particle Physics (CCAPP) Fellow.

© 2010 The Authors
Monthly Notices of the Royal Astronomical Society © 2010 RAS

ABSTRACT

We report the *Swift* discovery of the nearby long, soft gamma-ray burst GRB 100316D, and the subsequent unveiling of its low-redshift host galaxy and associated supernova. We derive the redshift of the event to be $z = 0.0591 \pm 0.0001$ and provide accurate astrometry for the gamma-ray burst (GRB) supernova (SN). We study the extremely unusual prompt emission with time-resolved γ-ray to X-ray spectroscopy and find that the spectrum is best modelled with a thermal component in addition to a synchrotron emission component with a low peak energy. The X-ray light curve has a remarkably shallow decay out to at least 800 s. The host is a bright, blue galaxy with a highly disturbed morphology and we use Gemini-South, Very Large Telescope and *Hubble Space Telescope* observations to measure some of the basic host galaxy properties. We compare and contrast the X-ray emission and host galaxy of GRB 100316D to a subsample of GRB-SNe. GRB 100316D is unlike the majority of GRB-SNe in its X-ray evolution, but resembles rather GRB 060218, and we find that these two events have remarkably similar high energy prompt emission properties. Comparison of the host galaxies of GRB-SNe demonstrates, however, that there is a great diversity in the environments in which GRB-SNe can be found. GRB 100316D is an important addition to the currently sparse sample of spectroscopically confirmed GRB-SNe, from which a better understanding of long GRB progenitors and the GRB-SN connection can be gleaned.

Key words: gamma-ray burst: individual: GRB 100316D – supernovae: individual: SN 2010bh.

1 INTRODUCTION

The connection between long-duration gamma-ray bursts (GRBs) and Type Ic core-collapse supernovae (SNe) has long been established, beginning with the association of GRB 980425 with SN 1998bw (Galama et al. 1998; Pian et al. 1998). Subsequent associations between nearby GRBs and spectroscopically confirmed SNe include GRB 030329/SN 2003dh (Hjorth et al. 2003; Stanek et al. 2003), GRB 031203/SN 2003lw (Malesani et al. 2004) and most recently GRB 060218/SN 2006aj (Campana et al. 2006; Pian et al. 2006). These are spectroscopically confirmed examples of nearby GRB-SN associations (out to $z = 0.17$). The characteristic 'bump' of an SN has been noted in the photometric data for a dozen or more GRBs out to $z \sim 1$ (e.g. Zeh Klose & Hartmann 2005; Della Valle et al. 2006; Ferrero et al. 2006; Woosley & Bloom 2006; Tanvir et al. 2010), while the majority of GRBs lie at higher redshifts where such signatures would be impossible to detect ($\langle z \rangle = 2.2$ Jakobsson et al. 2006; Fynbo et al. 2009). The GRBs with SNe are therefore rare, but provide a crucial insight into the GRB-SN connection and the progenitors of long GRBs.

The GRBs with spectroscopically confirmed SNe are generally underluminous and subenergetic in comparison to a typical long GRB, though GRB 030329 is a notable exception to this. The prompt emission of these bursts has a lower energy spectral peak than a typical GRB (Kaneko et al. 2007), and they are suggested to have less relativistic outflows or be viewed more off-axis. It has been suggested that the observed nearby ($z < 0.1$), underluminous/subenergetic GRBs, including GRB 100316D, may be drawn from a different population to the cosmological GRB sample, motivated by estimates of the local GRB rate several times greater than the rate of cosmological GRBs (e.g. Cobb et al. 2006; Chapman et al. 2007; Liang et al. 2007). Radio observations of GRBs suggest that mildly relativistic ejecta and often high luminosities are the properties that distinguish the supernovae associated with GRBs from the non-relativistic ordinary Type Ib/c SNe (Kulkarni et al. 1998; Soderberg et al. 2006).

GRB 060218 was a landmark long-duration, low-luminosity, soft spectral peak event, detected by the *Swift* satellite (Gehrels et al. 2004) with unprecedented multiwavelength coverage of the prompt emission. The prompt spectrum was found to comprise both the non-thermal synchrotron emission ascribed to most GRBs and thought to originate in the collision of fast-moving shells within the GRB jet (e.g. Rees & Mészáros 1994), and a thermal component. The presence of this thermal component, together with its evolution, led to the suggestion that we were observing the shock breakout of the SN for the first time (Campana et al. 2006; Waxman Mészáros & Campana 2007). However, the non-thermal emission did not differ greatly from that of the X-ray flash class of soft GRBs and an outflow speed close to the speed of light could be inferred (Toma et al. 2007), alternatively suggesting this to be an extension of the typical GRB population and not requiring significantly slower ejecta or any special (off-axis) geometry (Ghisellini Ghirlanda & Tavecchio 2007). Toma et al. (2007) speculate that the long-duration, low-luminosity events such as this one may point to a different central engine for these events compared with more typical GRBs: a neutron star rather than a black hole (see also Mazzali et al. 2006; Fan et al. 2010).

Also of relevance to this discussion are the SNe for which no GRB was detected, yet for which mildly relativistic ejecta provide a good explanation for the radio data: SN 2007gr (Paragi et al. 2010) and SN 2009bb (Soderberg et al. 2010). As GRB jets are thought to be highly collimated, it is expected that many will go undetected if the emission is directed away from our line of sight (e.g. Mazzali et al. 2005), and a fraction will also lie below current detector sensitivity limits. Soderberg et al. (2010) estimate the fraction of Type Ib/c SNe with central engines at about 1 per cent, consistent with the inferred rate of nearby GRBs. In contrast, there are nearby GRBs for which an accompanying SN could be expected but none has been detected to extremely deep limits. GRBs 060505 and 060614 (Della Valle et al. 2006; Fynbo et al. 2006; Gal-Yam et al. 2006) are the two best examples of this, highlighting the need for a greater understanding of the relationship between GRBs and SNe.

© 2010 The Authors, MNRAS **411,** 2792–2803
Monthly Notices of the Royal Astronomical Society © 2010 RAS

We present the discovery of a new GRB-SN, GRB 100316D (Stamatikos et al. 2010) associated with SN 2010bh (Bufano et al. 2010; Chornock et al. 2010; Wiersema et al. 2010). This is an unusually long-duration, soft-spectrum GRB positioned on a nearby host galaxy. Many of the properties of this GRB appear unlike those of typical GRBs, resembling rather GRB 060218. In this paper, we report accurate astrometry for the GRB-SN and the redshift of the underlying host galaxy. We examine the GRB prompt and afterglow emission observed with all three instruments on-board *Swift*, and the broad characteristics of the host galaxy as observed with the Gemini-South telescope, the Very Large Telescope (VLT) and the *Hubble Space Telescope* (*HST*). We compare these properties with the GRB sample as a whole and with a subset of GRB-SNe, to understand the origins of the GRB emission and further our knowledge of the GRB-SN connection.

2 OBSERVATIONS AND ANALYSES

2.1 *Swift*

On 2010 March 16 at 12:44:50 UT (hereafter T_0), the *Swift* Burst Alert Telescope (BAT; Barthelmy et al. 2005) triggered on and slewed immediately to GRB 100316D (Stamatikos et al. 2010). This was an image trigger, since no rapid, substantial rise in the count rate occurred, but a possible low-level peak of about 100 s long was noted in Stamatikos et al. (2010). The X-ray Telescope (XRT; Burrows et al. 2005) on-board *Swift* began observing the field at 12:47:08.1 UT, 137.7 s after the BAT trigger, beginning with 10 s of Windowed Timing (WT) mode settling data and followed by 593 s of WT pointing data. After a time gap due to observing constraints, data-taking recommenced at $T_0 + 33$ ks with XRT in Photon Counting (PC) mode. The best X-ray position for this source is the astrometrically corrected XRT position of RA, Dec. (J2000) = $07^{\rm h}10^{\rm m}30\overset{\rm s}{.}63$, $-56^{\rm d}15'19\overset{''}{.}7$, with an uncertainty of 3.7 arcsec (radius, at 90 per cent confidence; Starling Evans & Stamatikos 2010). *Swift's* UltraViolet-Optical Telescope (UVOT; Roming et al. 2005) began observing with the white filter 148 s after the BAT trigger and continued observations in the *u* band, thereafter cycling repeatedly through all its lenticular filters.

The *Swift* data were processed and analysed with the *Swift* tools version 3.5, released as part of HEASOFT 6.8, and the latest calibration data at 2010 March were used.

XRT WT spectra were grouped with a minimum of 20 counts in each bin, allowing the use of χ^2 statistics, while for the PC spectrum 1 count per bin was required and Cash statistics used. We fitted the X-ray spectra over the energy range of 0.3–10 keV and the γ-ray spectra over the range of 15–50 keV (as this is a soft event, very few counts are present above 50 keV) using the spectral fitting package XSPEC (Arnaud 1996). We used the X-ray absorption models PHABS and ZPHABS for which photoionization cross-sections were taken from Verner et al. (1996) and solar abundances from Wilms, Allen & McCray (2000). The Galactic absorption in the X-ray band is fixed at 7×10^{20} cm^{-2} throughout (Kalberla et al. 2005). We tested for any differences in the spectral fitting results from use of different grade selections or different energy ranges (excluding 0.3–0.5 keV and/or including 50–150 keV) and confirm that these have no effect.

Optical/UV photometry was performed with the UVOT tool UVOTSOURCE. At the position of the SN reported by Levan et al. (2010), background-subtracted count rates were extracted using a circular source aperture of 2.5 arcsec. Source-free background was taken from a region situated outside of the host galaxy. The count rate was aperture corrected to 5 arcsec in order to be compatible with the UVOT calibration (Poole et al. 2008). With UVOT we detect the host galaxy, but no new point sources. The 3σ upper limit on any optical transient emission was taken to be the background-subtracted count rate plus three times the count rate error and was converted into magnitude using the zero-points provided in Poole et al. (2008). At this time, galaxy subtraction cannot be performed since there are no UVOT pre- or post-explosion observations. The host galaxy count rate was determined using an elliptical source region, which enclosed the whole galaxy, and a source-free background region. Photometry of the host was performed on a sum of all data from $\sim 1 \times 10^5$ s after the trigger onwards for each filter. Since the ellipse is similar in area to a 5-arcsec circular aperture (semimajor and semiminor axes of 7.5 and 5.5 arcsec, respectively), we have taken the standard UVOT coincidence loss correction to be the best estimate of the coincidence loss, and the standard UVOT zero-points have been used to convert the count rate into magnitudes.

2.2 Gemini, VLT and *HST*

Our first optical observations of GRB 100316D were obtained with Gemini-South, starting on March 16 23:53 UT. In these images we identified two point sources, consistent with the initial XRT position (Vergani et al. 2010). We acquired spectroscopy of these with the three-arm echelle spectrograph X-shooter (D'Odorico et al. 2006), mounted on Unit Telescope 2 of the VLT. These sources were later shown to be compact H II regions unrelated to the SN. In this paper we will make use of the spectra obtained of the brightest of these two regions, referred to as source 'A' in Vergani et al. (2010) (see Fig. 1). We obtained two spectra, each of 1200-s exposure of source A, using a 5-arcsec nod throw along the slit to achieve better sky subtraction. We used slit widths of 1.0, 1.0 and 0.9 arcsec for the UVB, VIS and near-infrared (NIR) arms, respectively. Data were reduced using version 0.9.4 of the ESO X-shooter pipeline (Goldoni et al. 2006). Calibration data (bias, dark, arc lamp, flat-field and flexure control frames) were taken the same night. Extracted spectra were flux calibrated using spectrophotometric standard star exposures, also taken the same night, resulting in flux-calibrated spectra spanning the ultraviolet to the near-infrared ($\sim$300–2300 nm) simultaneously.

We obtained further imaging of the localization with Gemini-South on the subsequent three nights; using these, we were able to identify a further bright point source superimposed on the host galaxy (Levan et al. 2010). Image subtraction performed between the different images showed a clear brightening in this source, which we subsequently identified as the associated rising SN (Wiersema et al. 2010; Fig. 1).

We obtained deep imaging of the position of GRB 100316D using the Focal Reducer and Spectrograph 2 (FORS2) instrument on Unit Telescope 1 of the VLT. Seeing conditions during both epochs were good, averaging 0.8 arcsec, but the second epoch observations suffer from a fairly bright background caused by high airmass and a bright moon. The GRB-SN is clearly visible in both epochs.

Following the announcement of an SN discovery (Wiersema et al. 2010), we triggered our cycle 17 *HST* programme. Here we report the first epoch, obtained on March 25, $\sim$9 d after the BAT trigger.

The details of the ground-based and *HST* observations are given in Table 1. The data were reduced using standard procedures in IRAF.

3 ASTROMETRY AND REDSHIFT

Subtraction of early from late images taken with Gemini-South reveals a variable source inside the X-ray error circle which we

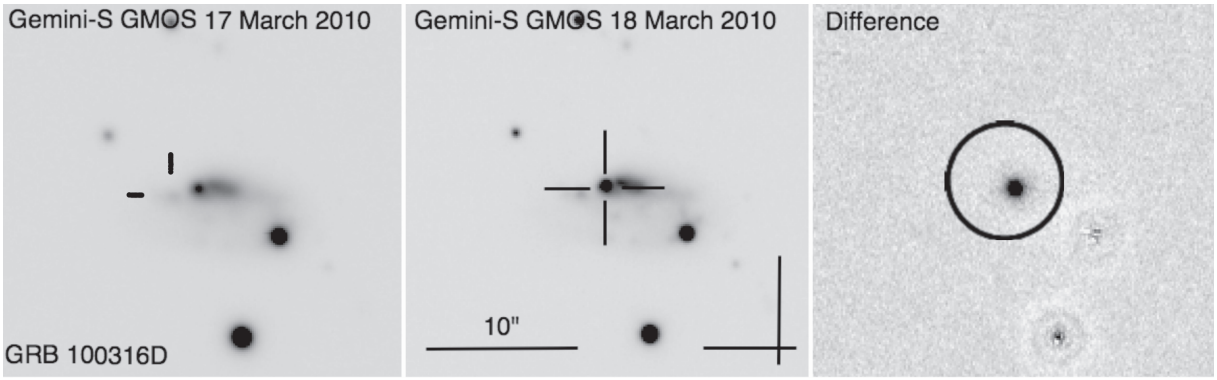

Figure 1. Our Gemini-South discovery images of SN 2010bh, associated with GRB 100316D. The *r*-band images, obtained one night apart, clearly show the afterglow/SN superimposed on its host light. The GRB/SN position, image scale and north and east directions are indicated in the middle panel. The star-forming region 'A' is indicated in the left-hand panel. The result of PSF-matched image subtraction is shown in the right-hand panel, revealing a brightening of the transient. The *Swift* XRT error circle is overlaid on this panel.

Table 1. Log of Gemini-South, VLT and *HST* observations.

Date start (UT)	Telescope/instrument + filter/arm	$T_{\rm exp}$ (s)	Comments
2010-03-16, 23:53	Gemini-S/GMOS *r*	5 × 180	
2010-03-17, 00:58	VLT/X-shooter UVB+VIS+NIR	2 × 1200	Region A
2010-03-17, 23:55	Gemini-S/GMOS *r*	5 × 180	
2010-03-18, 23:48	Gemini-S/GMOS *r*	5 × 180	
2010-03-20, 00:28	Gemini-S/GMOS *griz*	3 × 60	
2010-03-24, 00:07	VLT/FORS2 $R_{\rm special}$	180	
	VLT/FORS2 $I_{\rm Bessel}$	180	
	VLT/FORS2 $V_{\rm high}$	180	
2010-03-25, 04:38	HST/WFC3/UVIS *F555W*	2 × 60	
2010-03-29, 01:11	VLT/FORS2 $V_{\rm high}$	6 × 150	SN saturated
	VLT/FORS2 $R_{\rm special}$	17 × 50	
	VLT/FORS2 $I_{\rm Bessel}$	9 × 75	
	VLT/FORS2 $V_{\rm high}$	17 × 50	

conclude is GRB 100316D/SN 2010bh (Fig. 1). We find an accurate position for this variable source by astrometrically calibrating the images, using 190 United States Naval Observatory B (USNO-B) catalogue stars in the field. We determine the position of the residual in the image subtraction by using a Gaussian centroiding. This gives a position for the SN of RA, Dec. (J2000) = $07^{\rm h}10^{\rm m}30\overset{\rm s}{.}558$, $-56^{\rm d}15'20\overset{''}{.}18$ ($\pm$0.26 arcsec). The error is dominated by the scatter of the USNO positions around the best-fitting polynomial of the astrometric calibration. We refine this using an image taken with *HST*, to our best position of RA, Dec. (J2000) = $07^{\rm h}10^{\rm m}30\overset{\rm s}{.}530$, $-56^{\rm d}15'19\overset{''}{.}78$ ($\pm$0.05 arcsec).

We detect a large number of nebular emission lines commonly found in star-forming regions with a good signal-to-noise ratio in the VLT X-shooter spectrum of source A (see Section 7, Fig. 5). From the 12 brightest lines, we measure the redshift $z = 0.0591 \pm 0.0001$. Using the cosmology $\Omega_{\rm M} = 0.27$, $\Omega_\Lambda = 0.73$ and $H_0 = 71$ km s^{-1} Mpc^{-1}, the luminosity distance is 261 Mpc.

4 TEMPORAL CHARACTERISTICS OF THE PROMPT EMISSION

The BAT and XRT early emission light curves are shown in Fig. 2. The γ-ray emission was detected at the 10σ level at T_0 −475 s, prior to which there was no detected emission at 5σ or above. The emission peaked at T_0 −100 s and decayed with an exponential decay constant of 750 s. Emission continued through the slew at $T_0 + 750$ s. BAT reobserved at $T_0 + 5050$ s from which time γ-ray emission was no longer detected.

The prompt emission duration of this GRB is one of the longest ever measured. GRB 100316D was detected with BAT from $\sim T_0 - 500$ s to at least $\sim T_0 + 800$ s; hence, the lower limit on the duration of GRB 100316D is ∼1300 s. The fluence, derived from the 15–150 keV spectrum accumulated between $T_0 - 475.0$ and $T_0 + 795.0$ s since trigger, is $S_\nu = (5.10 \pm 0.39) \times 10^{-6}$ erg cm^{-2}. We note that as γ-ray emission continued after this time but *Swift* was unable to observe, this should be considered a lower limit to the burst fluence. The isotropic equivalent energy that follows from this is $E_{\rm iso} \geq (3.9 \pm 0.3) \times 10^{49}$ erg. This is valid for the energy range of 15–150 keV, but if we extrapolate down to 1 keV given that this is a soft burst, we find that the fluence and therefore $E_{\rm iso}$ may be higher by 50 per cent leading to $E_{\rm iso} \geq (5.9 \pm 0.5) \times 10^{49}$ erg. We note that little flux is observed above 50 keV; the contribution to the isotropic energy from very high energy γ-rays is likely to be small.

The BAT and XRT simultaneous coverage spans 603 s. The XRT count rate light curve decays very slowly with $\alpha = 0.13 \pm 0.03$ throughout this interval.

© 2010 The Authors, MNRAS **411,** 2792–2803
Monthly Notices of the Royal Astronomical Society © 2010 RAS

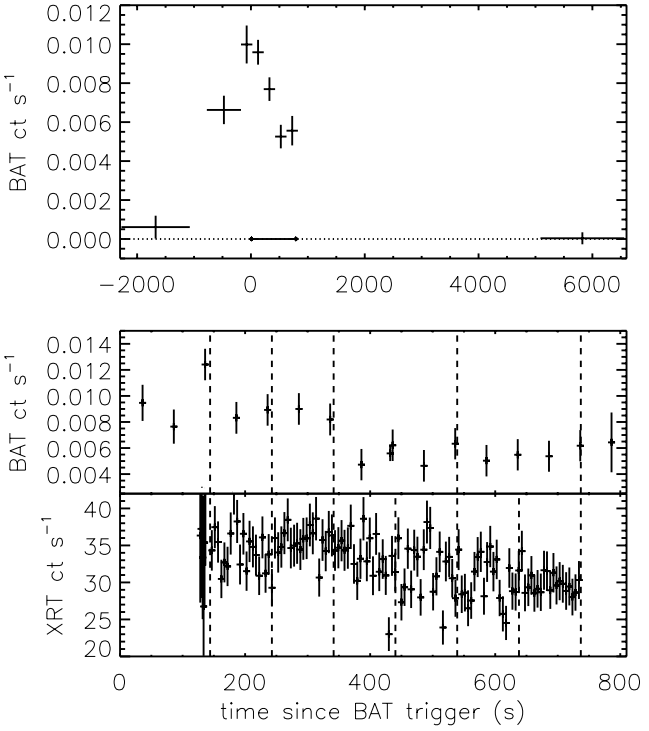

Figure 2. Top panel: 14–195 keV long-term BAT light curve, comprising both event and survey binned data. The zero count-rate level is indicated with a dashed line, and the time range covered by the panels below is overlaid as a double-sided arrow. Bottom two panels: zoom in on the 14–195 keV BAT event light curve and the 0.3–10 keV XRT light curve from T_0 to $T_0 +$ 810 s. The dashed lines indicate time slices adopted for spectral fitting.

Table 2. UVOT 3σ upper limits on the magnitude at the position of the SN, from event and image data. We note that these are background subtracted but not host subtracted. The time ranges were chosen to overlap with the simultaneous BAT-XRT coverage.

Filter	$T_{\rm mid}$ (s since BAT trigger)	$T_{\rm exp}$ (s)	Magnitude
White	195	93	>21.3
	270	54	>21.0
	597	19	>20.3
v	647	19	>18.4
b	650	22	>19.6
u	324	35	>19.3
	440	194	>20.6
	634	36	>19.4
*uvw*1	696	19	>18.2
*uvm*2	671	19	>17.6

No variable optical or UV source has been detected during *Swift* observations with the UVOT, hampered by the bright underlying host galaxy (Oates De Pasquale & Stamatikos 2010). The light curves for each filter are consistent with a constant value, and we confirm that no variable source is detected with image subtraction using the full UVOT data set to date. Upper limits on the magnitudes of any source at the GRB position are given in Table 2.

5 SPECTRAL CHARACTERISTICS OF THE PROMPT EMISSION

We have carried out time-resolved spectroscopy during the 593 s of BAT-XRT overlap from $T_0 + 144$ s to $T_0 + 737$ s. For the X-ray data, we take six consecutive time slices, each of ∼99 s duration. We fit an absorbed power-law model and then include a further blackbody component (Fig. 3). In either case, the X-ray spectral shape appears stable throughout the WT observations. The intrinsic absorption measured in both sets of fits is consistent at each epoch. We then fit the time-averaged WT spectrum consisting of data from $T_0 +$ 144 to $T_0 + 737$ s since trigger to obtain the best constraints on the intrinsic column which we use in the following BAT-XRT joint fits. The time-averaged WT spectrum and the time-sliced WT spectra are adequately fitted with an absorbed power-law model; however, the inclusion of a blackbody provides a significant improvement in the fits (F-test probabilities of 10^{-10} and 10^{-6}, respectively), requiring a larger intrinsic absorption column to accommodate a $kT = 0.14 \pm 0.01$ keV blackbody component while the power-law photon index remains approximately the same. The blackbody component contributes ∼3 per cent of the total 0.3–10 keV X-ray flux in this model and has a luminosity of (3–4) $\times$ 10^{46} erg s^{-1} corresponding to an emitting radius of 8×10^{11} cm. The blackbody luminosity and temperature (Fig. 4) are consistent with remaining constant until at least $T_0 + 800$ s.

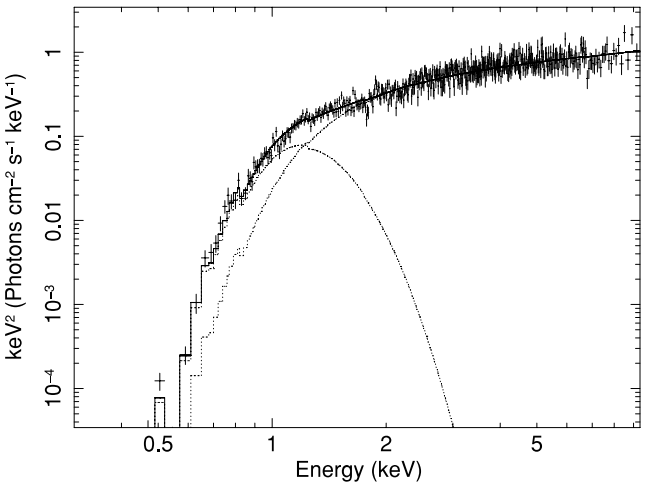

Figure 3. Unfolded XRT WT time-averaged spectrum, EF_E versus E, with an absorbed power-law plus blackbody model, showing the contributions of the two components.

In order to more rigorously test the significance of the blackbody component, we simulated 10 000 spectra based on the absorbed power-law model that best fits the time-averaged WT spectrum of GRB 100316D (Table 3). We fitted the simulated spectra with absorbed power-law plus blackbody models to recover the chance probability that adding a blackbody component significantly improves the fit, following the methodology described in Hurkett et al. (2008). There were no simulated spectra for which $\Delta\chi^2$ indicated an improvement in the fit comparable to that found in our data, implying that the blackbody component in the time-averaged WT spectrum of GRB 100316D is >4σ significant. This test gives us a high degree of confidence in our identification of a thermal component in the X-ray spectrum at early times.

The joint BAT-XRT fits were performed with two 99-s and two 198-s consecutive time slices. We fit these spectra with an exponentially cut-off power-law model[1] with and without a blackbody component. A constant normalization ratio of the BAT to XRT spectra (to account for calibration uncertainties in the response matrices

[1] Defined as $A(E) = E^{-\Gamma} e^{-E(2-\Gamma)/E_{\rm pk}}$.

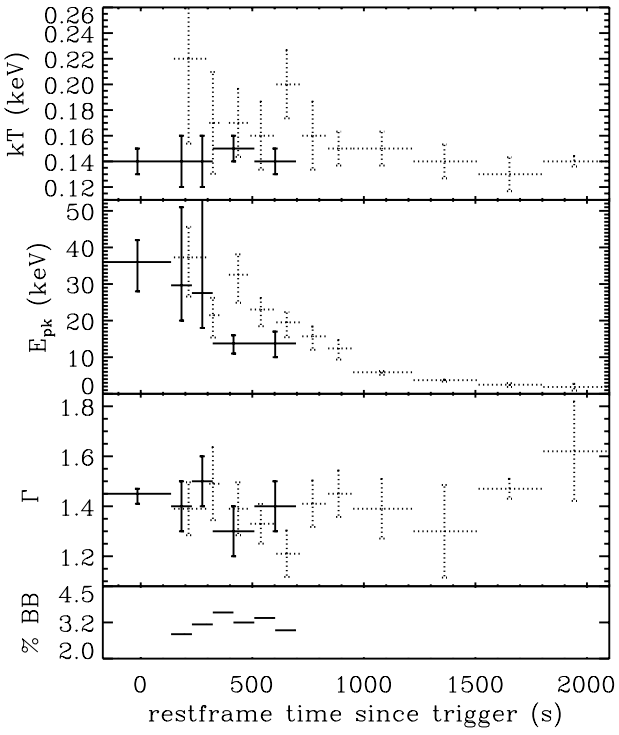

Figure 4. Evolution of power-law photon index Γ, peak energy $E_{\rm pk}$ and blackbody temperature kT in the blackbody plus exponentially cut-off power-law model fitted to the BAT-XRT spectra for GRB 100316D (solid error bars), compared with the same model fitted to BAT-XRT data of GRB 060218 (taken from Kaneko et al. 2007, dotted error bars) in the source rest frames. Errors are 90 per cent confidence. The bottom panel shows the percentage contribution of the blackbody component to the total observed 0.3–10 keV X-ray flux, in time-sliced XRT spectral fits to GRB 100316D.

of the different instruments) is not included in the reported fits since we found this to be 0.9 ± 0.2, i.e. consistent with unity. The exponentially cut-off power-law model provides a good fit with a stable low energy power-law slope of $\Gamma \sim 1.4$. The peak energy is at $\sim$30 keV in the first time interval and moves to lower energies with time (Fig. 4). To estimate the spectral shape during and prior to the BAT trigger, we fitted the BAT spectrum from $T_0 - 175$ to $T_0 + 144$ s simultaneously with the time-averaged WT spectrum, given that no significant X-ray spectral evolution is observed in the interval 144–737 s. We stress that because the data are not simultaneous, this fit provides only an indication of the spectral shape at early times. Spectral fitting results are given in Table 3.

The latest time slice taken for our joint BAT-XRT fits also has full coverage in the u band with UVOT. We have included the u-band 3σ upper limit and refitted the data with an absorbed and reddened blackbody+power-law model. We obtain an acceptable fit, when the underlying spectrum is fixed in shape as listed in Table 3, with an intrinsic extinction of $E(B-V) \sim 0.9$ mag or $A_v \sim 2.6$ mag using the Small Magellanic Cloud extinction law [Pei 1992; fixing the Galactic extinction to $E(B-V) = 0.12$ mag according to Schlegel, Finkbeiner & Davis 1998]. This provides a lower limit on the host galaxy extinction along the line of sight to the GRB, only under the assumption that any optical transient emission lies on an extrapolation of the high energy spectrum. A measurement of the optical extinction along the line of sight to the GRB can be made with spectroscopy of the SN, for example through the strength of interstellar medium Na I lines (Bufano et al., in preparation).

6 THE LATE-TIME BEHAVIOUR

The X-ray emission after 10^4 s decayed more steeply than did the emission during the first 800 s after the BAT trigger. Treating the early and late X-ray emission separately, we fit only the data after 10^4 s with a power-law decay. This results in an acceptable fit, with $\alpha = 1.35 \pm 0.30$.

The XRT count rates for this source lie within the spread of the entire XRT GRB light-curve sample at all observed times; however, its shape is atypical. Four light-curve types were identified in the *Swift* XRT catalogue, to which 76 per cent of their sample could be ascribed (Evans et al. 2009). GRB 100316D appears not to fit any of these light-curve types, if all the early data are included.

The X-ray spectrum from $T_0 + 3 \times 10^4$ to 5×10^5 s allows only poor constraints on the parameters of an absorbed power-law model, but we find that it is significantly spectrally softer at this time than in the earlier WT data. Using Cash statistics, and fixing the intrinsic absorption to that found in the combined WT spectrum, we find that the power law has a photon index of $\Gamma = 3.5 \pm 1.0$ (Table 3). This is a very high value, or a very soft spectrum, that although not unique among *Swift* bursts (see e.g. Evans et al. 2009) is difficult to accommodate within the standard fireball model generally used to explain GRB afterglow emission (e.g. Sari, Piran & Narayan 1998), but may possibly be explained with inverse Compton scattering (e.g. Waxman, Mészáros & Campana 2007). The temporal decay rate, however, is rather typical of GRB afterglows.

We now turn to the optical regime, to estimate the SN contribution at the epochs of our VLT data. We performed point spread function (PSF) matched image subtraction on the FORS2 images, using the ISIS2 code (Alard 2000). For the second epoch $V_{\rm high}$ data we use the short exposure time images, as the frames with longer exposure time show the SN to be somewhat saturated. The subtraction shows a residual at the position of the SN associated with this GRB (Wiersema et al. 2010) in the V and I bands, whereas the subtraction is too noisy in the R band. This residual shows that the SN is fainter in the second FORS2 epoch than in the first epoch, at least in V and I, suggesting that the SN peaked in these bands between 8 and 13 d after burst. This is similar to the SN 2006aj (GRB 060218), which peaked at 10.2 ± 0.3 d after burst in V (Ferrero et al. 2006; Mirabal et al. 2006; Modjaz et al. 2006; Sollerman et al. 2006).

7 THE HOST GALAXY

The deep Gemini, VLT and *HST* observations show a bright, blue galaxy, covering the 3.7-arcsec radius refined XRT error circle (Figs 1 and 8). The galaxy has a highly disturbed morphology, but is dominated by a central bright region, possibly the galaxy nucleus, and an arc-like shape resembling a spiral arm. The galaxy hosts a large number of knots, or blobs, likely giant H II regions. Colour differences between these knots can be discerned, caused by differences in age, metallicity, reddening or a combination of these. The SN itself is located on top of a bright, blue knot, close (in projection) to the possible galaxy nucleus. The UVOT also observed the host galaxy in all filters and approximate magnitudes, uncorrected for extinction and including an unknown level of contamination by the afterglow and/or SN, are reported in Table 4.

It has long been contended that the properties of the host galaxies of GRBs can provide additional clues to the progenitor evolution, through determination of properties such as the age, metallicity and alpha element enrichment of the stellar population. The low-redshift GRB-SNe are of particular interest, as they allow one to obtain spatially resolved spectroscopy (e.g. Christensen et al. 2008).

Table 3. Spectral fits to the *Swift* BAT and XRT data with an absorbed power law (PL) or a cut-off power law (CPL) model, with and without a blackbody (BB) component. Errors are quoted at the 90 per cent confidence level. Galactic absorption is fixed at 7×10^{20} cm^{-2}.

	PL or CPL			PL+BB or CPL+BB			
T (s since BAT trigger)	$N_{\rm H,int}$ (10^{22} cm^{-2})	Γ	$E_{\rm pk}$ (keV)	$N_{\rm H,int}$ (10^{22} cm^{-2})	kT (keV)	Γ	$E_{\rm pk}$ (keV)
XRT WT time-averaged:		$\chi^2/\nu = 587.9/480$			$\chi^2/\nu = 538.8/478$		
144–737	0.91 ± 0.05	$1.40^{+0.04}_{-0.03}$	–	1.83 ± 0.06	0.14 ± 0.01	1.53 ± 0.06	–
XRT WT time-sliced:		$\chi^2/\nu = 830.9/754$			$\chi^2/\nu = 782.1/742$		
144–243	0.90 ± 0.05^a	1.35 ± 0.06	–	1.8 ± 0.2^a	0.14 ± 0.02	1.5 ± 0.1	–
243–342	0.90 ± 0.05^a	1.41 ± 0.06	–	1.8 ± 0.2^a	0.14 ± 0.02	1.6 ± 0.1	–
342–440	0.90 ± 0.05^a	1.36 ± 0.06	–	1.8 ± 0.2^a	0.15 ± 0.02	1.5 ± 0.1	–
440–539	0.90 ± 0.05^a	1.43 ± 0.06	–	1.8 ± 0.2^a	$0.14^{+0.03}_{-0.02}$	1.6 ± 0.1	–
539–638	0.90 ± 0.05^a	1.43 ± 0.06	–	1.8 ± 0.2^a	0.13 ± 0.02	1.5 ± 0.1	–
638–737	0.90 ± 0.05^a	1.40 ± 0.06	–	1.8 ± 0.2^a	$0.14^{+0.03}_{-0.02}$	1.6 ± 0.1	–
XRT PC time-averaged:		C-statistic/$\nu = 13.8/15$			C-statistic/$\nu = 15.4/15$		
32906–508263	0.90 fixed	3.5 ± 1.0	–	1.83 fixed	–	$4.6^{+1.6}_{-1.3}$	–
BAT:		$\chi^2/\nu = 16.0/14$					
−175 to 144	–	2.1 ± 0.4	–				
BAT-XRT:		$\chi^2/\nu = 617.4/518$			$\chi^2/\nu = 572.1/516$		
−175 to 144[b]	0.90 fixed	1.33 ± 0.03	33^{+7}_{-5}	1.83 fixed	0.14 ± 0.01	$1.45^{+0.02}_{-0.04}$	34^{+8}_{-6}
BAT-XRT:		$\chi^2/\nu = 853.4/768$			$\chi^2/\nu = 806.1/760$		
144–243	0.90 fixed	1.25 ± 0.08	25^{+9}_{-5}	1.83 fixed	0.14 ± 0.02	1.4 ± 0.1	28^{+23}_{-8}
243–342	0.90 fixed	1.32 ± 0.08	22^{+9}_{-5}	1.83 fixed	0.14 ± 0.02	1.5 ± 0.1	26^{+36}_{-8}
342–539	0.90 fixed	$1.24^{+0.06}_{-0.07}$	14^{+3}_{-2}	1.83 fixed	0.15 ± 0.01	1.3 ± 0.1	13^{+3}_{-2}
539–737	0.90 fixed	1.28 ± 0.07	14 ± 3	1.83 fixed	0.14 ± 0.01	1.4 ± 0.1	13^{+4}_{-3}

[a]These parameters are tied together for all time intervals. [b]XRT data are not available during this time. We perform this fit only to provide an indication of the cut-off power law parameters over this time interval, using the time-averaged WT spectrum given that no significant X-ray spectral evolution is detected in the interval 144–737 s. Therefore, this fit was performed separately rather than simultaneously with the 144–737 s interval BAT-XRT time-sliced fits.

Table 4. UVOT-observed magnitudes and 1σ errors for the host galaxy. Photometry is performed as described in Section 2.1. Note that any afterglow or SN contribution is uncertain and so it cannot be removed; however, no variability is seen in subtraction of late-time images from earlier epochs.

Filter	$T_{\rm start}$ (s since BAT trigger)	$T_{\rm stop}$ (s since BAT trigger)	$T_{\rm exp}$ (s)	Magnitude
v	1.1×10^5	6.1×10^5	3229	17.71 ± 0.03
b	1.1×10^5	6.1×10^5	3578	18.29 ± 0.03
u	1.1×10^5	6.1×10^5	4325	18.02 ± 0.03
$uvw1$	1.1×10^5	6.3×10^5	8851	18.07 ± 0.03
$uvm2$	1.1×10^5	6.1×10^5	8332	17.99 ± 0.03
$uvw2$	1.1×10^5	6.1×10^5	16 226	18.00 ± 0.02

The derived properties can then be meaningfully compared to those of 'normal' core-collapse SN hosts (Fruchter et al. 2006; Svensson et al. 2010) or other star-forming galaxy populations. For these reasons, we analyse the X-shooter spectrum we obtained of a bright H II region within the host, which we call source A (Vergani et al. 2010), spatially distinct from the SN region (Figs 1 and 8). We choose to use this spectrum rather than the X-shooter spectra of the SN itself, as in these spectra the contribution of the SN to the spectrum is large and cannot be easily separated from the underlying H II region lines. Source A is located near the SN (projected distance of approximately 2 kpc), and we may expect the properties of this region to give a meaningful insight into the properties of the host as a whole.

We detect a large number of nebular emission lines commonly found in star-forming regions; a selection of those used here (which are all unresolved) is shown in Fig. 5. We use the Balmer Hα and Hβ line fluxes to measure a value for the Balmer decrement (jointly fitting the stellar Balmer absorption component and the nebular emission-line component), assuming case B recombination (e.g. Osterbrock 1989; Izotov, Thuan & Lipovetsky 1994). Assuming an electron temperature of 10^4 K, we compute the extinction [we find $E(B-V) = 0.178$ mag for the combination of Galactic reddening of $E(B-V)_{\rm gal} = 0.07$ mag and intrinsic reddening in source A] and deredden the spectrum accordingly.

We compute the average electron density $n_{\rm e}$ using the [S II] doublet and the [O II] doublet: both of the doublet flux ratios are consistent with their lower limits, so we assume a value of $n_{\rm e} = 100$ cm^{-3} (see e.g. Osterbrock 1989). The electron temperature sensitive [O III] λ4363 and [O II] $\lambda\lambda$7320,7331 doublets are detected, from which we calculate the electron temperatures for O^{2+} and O^+ directly (e.g. Osterbrock 1989), at $11\,880 \pm 800$ and $10\,400 \pm 1100$ K, respectively (errors are 1σ). Ionization corrections to account for the presence of O^{3+} were found to be negligible, also evidenced by the non-detection of He II λ4686, so we determine the oxygen abundance in region A as $O/H = O^+/H^+ + O^{2+}/H^+$. Using the measured line fluxes, densities and temperatures, we arrive at an electron temperature-based oxygen abundance of $12 + \log(O/H) = 8.23 \pm 0.15$ in region A [0.37 times solar metallicity, assuming a solar oxygen abundance of $12 + \log(O/H) = 8.66$; Asplund et al. 2004]. We note that a similar oxygen abundance has been derived from spectra at the SN site (see Chornock et al. 2010).

In the spectrum, we detect Balmer absorption lines underlying the nebular emission. This is common in GRB host galaxy spectra and can provide a useful age tracer, provided the spectra have

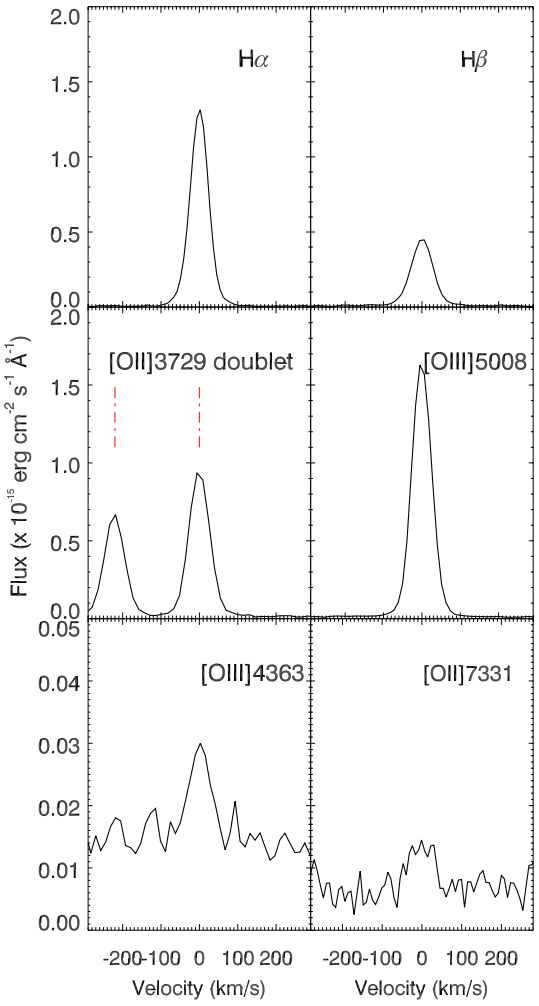

Figure 5. A selection of emission lines which are most important for the oxygen abundance analysis, detected in the X-shooter spectrum of the source 'A' H II region in the host galaxy, ∼2-kpc projection from the GRB/SN location. The top panels show the Balmer Hα and Hβ lines used for the determination of the reddening. The middle panels show the strong lines of the [O II] $\lambda\lambda$3727,3729 doublet and [O III] λ5008. The zero velocity point for [O II] $\lambda\lambda$3727,3729 is (arbitrarily) chosen to be the centre of the redmost component of the doublet. The bottom panels show the temperature sensitive lines of [O III] and [O II] (of the latter, only one member of the doublet is shown) from which we derive $T_e(O^{2+})$ and $T_e(O^+)$, respectively.

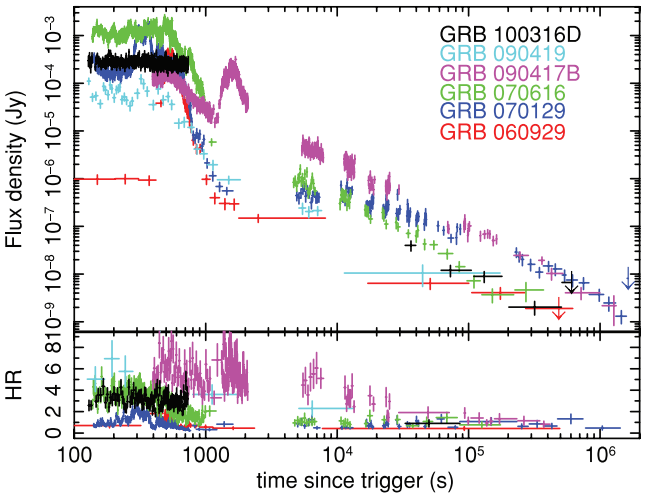

Figure 6. Top panel: X-ray light curves in flux density at 1.7 keV against time since trigger for a selection of *Swift* XRT-observed very long prompt emission duration (>400 s) GRBs (excluding 060218). Bottom panel: (1.5–10 keV)/(0.3–1.5 keV) hardness ratios derived from the XRT count rate light curves.

8 DISCUSSION

GRB 100316D is an atypical GRB both in its temporal and its spectral behaviour. The very soft spectral peak and extended and slowly decaying flux emission are highly unusual among the prompt emission of GRBs (e.g. Sakamoto et al. 2008). The estimated total isotropic energy [$E_{\rm iso} \geq (5.9 \pm 0.5) \times 10^{49}$ erg], when considered with the 90 per cent confidence range of spectral peak values of 10–42 keV we measure in Section 5, places GRB 100316D on the low $E_{\rm iso}$–low $E_{\rm pk}$ tail of the Amati correlation which relates $E_{\rm pk}$ and $E_{\rm iso}$ for the majority of typical GRBs (Amati 2006). The notable outlier to this relation is GRB 980425 (SN 1998bw) (e.g. Amati et al. 2007; Kaneko et al. 2007). We also compare this GRB with the relation reported by Gehrels et al. (2008) between the XRT flux at 11 h [here, $(3.2 \pm 0.8) \times 10^{-13}$ erg cm^{-2} s^{-1}] and BAT fluence and find, using the lower limit to the fluence, that it lies along the correlation with values that are typical for the sample of *Swift* GRBs reported in Evans et al. (2009).

GRB 100316D is among the longest duration *Swift* GRBs ($T_{90} \geq$ 1300 s), after GRB 090417B ($T_{90} \sim$ 2130 s) and GRB 060218 ($T_{90} \sim$ 2100 s). GRBs with durations of 400 s or longer, as quantified using the T_{90} parameter, account for only 1.4 per cent of the *Swift* sample observed to date. Owing to their long prompt emission durations, these GRBs are more likely to have exceptional broad-band coverage, lending themselves to prompt emission studies. We show the X-ray light curve and hardness ratio of GRB 100316D in relation to the T_{90} >400 s XRT-observed *Swift* events in Fig. 6 (omitting GRB 060218 as it can be seen in Fig. 7; data are taken from the *Swift* XRT GRB light-curve repository;[2] Evans et al. 2007).

This category comprises a number of different light-curve types, from those which are long due to triggering on a precursor or the presence of a broad flare to the very gradually decaying prompt emission of GRB 100316D. The *Swift* subsample shown here indicates two GRBs, in addition to GRB 060218, whose emission resembles GRB 100316D both in temporal decay and in spectral hardness: GRBs 070616 (Starling et al. 2008) and 090419 (Stratta

sufficient resolution (e.g. Wiersema, in preparation). We fit the Hδ absorption component and find an approximate age for the dominant stellar population of ∼30 Myr, assuming continuous star formation (Gonzalez Delgado, Leitherer & Heckman 1999). We also note the absence of obvious Wolf–Rayet star emission-line features in source A. The detection of the bright Hα line allows us to estimate the star formation rate (SFR) at location A: the Hα line luminosity is a tracer of recent star formation frequently used in nearby GRB host galaxies. We use the expression $SFR_{\rm H\alpha} = 7.9 \times 10^{-42} L_{\rm H\alpha}$ (Kennicutt 1998). Using the dereddened flux from the X-shooter spectrum, we find $SFR_{\rm H\alpha} = 0.17\,{\rm M}_\odot\,{\rm yr}^{-1}$. Note that no aperture correction is performed, so this value is formally a lower limit.

A more detailed analysis of the host galaxy will appear in Flores et al. (in preparation).

[2] http://www.swift.ac.uk/xrt_curves/

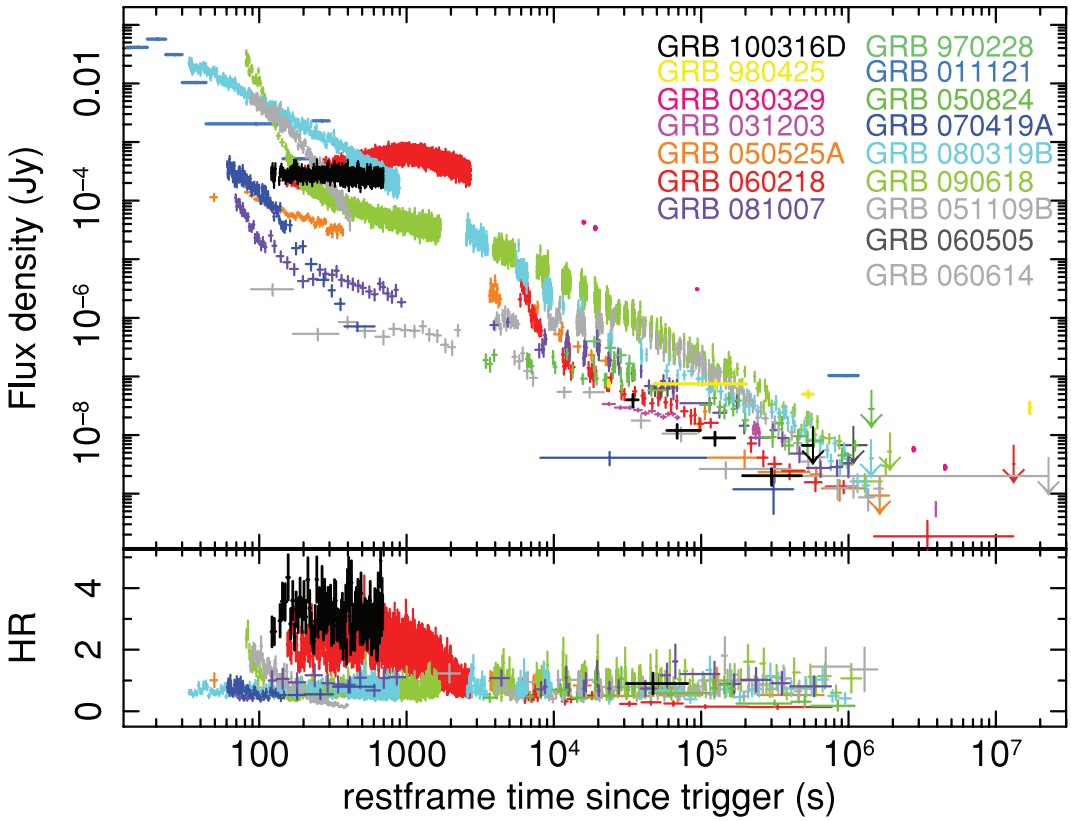

Figure 7. The top panel shows X-ray light curves against time since trigger in flux density at 1.7 keV for a selection of long GRBs with associated SNe (either spectroscopically confirmed – coloured in shades of red with GRB 100316D in black, or photometrically determined – shades of blue and green), two nearby long GRBs with no observed SNe to deep limits and a further long GRB likely at $z \leq 0.1$ with no reported SN (grey shades). The bottom panel shows the hardness ratios for the *Swift* XRT-observed GRBs, derived from the 1.5–10 keV and 0.3–1.5 keV count rate light curves in the same colour scheme. References for the data sources: 100316D (see footnote 2), 980425 (Pian et al. 2000), 030329 (Willingale et al. 2004), 031203 (Watson et al. 2004), 050525A (Blustin et al. 2006 and footnote 2), 060218 (see footnote 2), 081007 (see footnote 2), 970228 (Costa et al. 1997; De Pasquale et al. 2006), 011121 (Piro et al. 2005), 050824 (see footnote 2), 070419A (see footnote 2), 080319B (see footnote 2), 090618 (see footnote 2), 051109B (see footnote 2), 060505 (see footnote 2), 060614 (see footnote 2).

et al. 2009). We note that GRB 090417B is also spectrally hard at early times, but this may be attributed to strong X-ray flaring (Holland et al. 2010).

GRB 070616 was particularly well sampled, with γ-ray through optical coverage at early times clearly showing the movement of the spectral peak energy of the Band function (Band et al. 1993) and the occurrence of additional spectral softening (Starling et al. 2008). However, the spectrum was much harder than that of 100316D – observed by both *Swift* BAT and *Suzaku* Wide-band All-sky Monitor (WAM), and neither the redshift nor the presence of any SN could be established as the source lay close to a bright star.

We now discuss the properties of GRB 100316D in the context of GRB-SNe, paying particular attention to GRB 060218.

8.1 Comparison to GRBs with accompanying supernovae: high energy emission

In Fig. 7, we show the X-ray light curves and hardness ratios of a subset of the GRBs with associated SNe (either spectroscopically or photometrically confirmed). On this plot we also include GRB 051109B which was tentatively associated with a very low-redshift ($z = 0.08$; Perley et al. 2006) host galaxy and has no reported SN that we are aware of, and the well-studied nearby GRBs 060505 and 060614 for which SN searches to very deep limits registered no detections (Della Valle et al. 2006; Fynbo et al. 2006; Gal-Yam et al. 2006). The prompt emission shows a broader range of observed fluxes than the late-time decays, perhaps suggesting that they are unrelated or that an extra component is present in the early emission which contributes differently in each GRB. The majority of the GRB-SNe (and GRBs without SNe shown here) light curves decay steeply over the first 1000 s, with GRBs 100316D and 060218 being the only exceptions. The hardness ratios reveal that GRBs 100316D and 060218 have a similar spectral hardness evolution, clearly different from those of most other GRB-SNe which remain at a stable and softer spectral shape throughout the prompt and late-time emissions. GRBs 060614 (without an SN) and 090618 (photometrically discovered SN) also transition from hard to soft, but do this earlier, over the first 200 s during their steep decays. We note, however, that X-ray data during the early emission for a number of the GRB-SNe, including the spectroscopically confirmed GRB-SNe 980425, 030329, 031203 and 050525A, are either not available or inadequate for spectral studies.

8.2 Comparison to GRBs with accompanying supernovae: host galaxies

Nearby GRBs show a large variety in their host galaxy properties: the prototype GRB-SN, GRB 980425 and SN 1998bw, occurred in

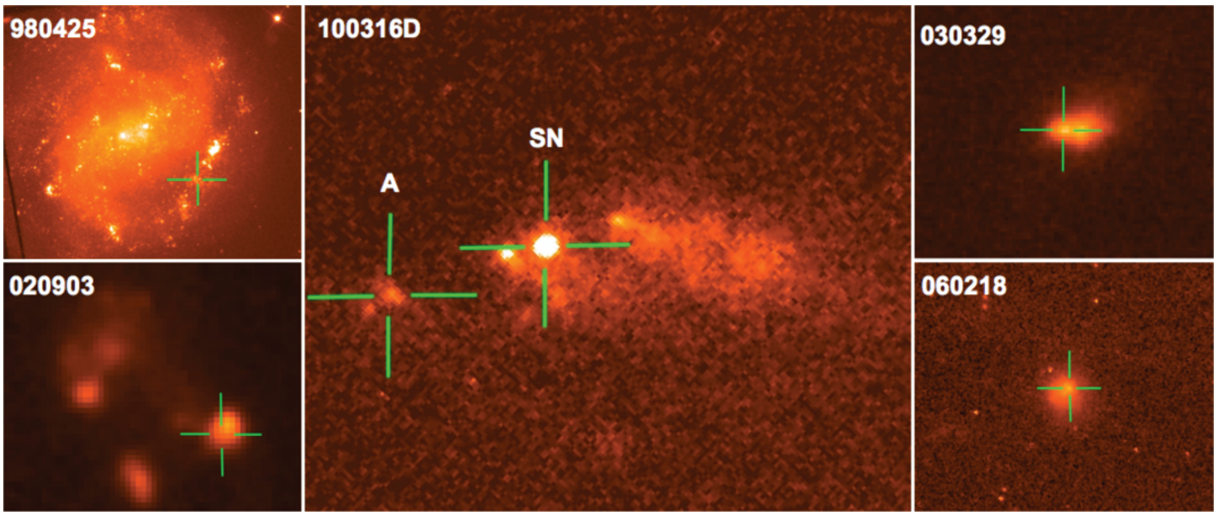

Figure 8. A mosaic of the host galaxies of spectroscopically confirmed SNe, associated with GRBs and imaged by the *HST*. The centre image shows the host of GRB 100316D, while other examples are shown in smaller insets. The physical scale across each image is approximately 7 kpc, and the positions of source A and of the SN are marked with crosshairs. Note that in the cases of GRB 060218 and 100316D, there is still some contamination from the SN at the time of the image.

Table 5. Host galaxies of nearby GRB-SNe. The absolute magnitudes M_B were taken from the compilation of Levesque et al. (2010).

GRB	T_e oxygen abundance [12 + log(O/H)]	Host type	Absolute magnitude M_B	References
980425	8.25 (GRB site) 8.39 (nearby WR region)	Dwarf spiral	−17.6	Sollerman et al. (2005) and Hammer et al. (2006)
020903	7.97	Irr	−18.8	Hammer et al. (2006)
030329	7.72	Irr	−16.5	Levesque et al. (2010)
031203	8.02 ± 0.15 (integrated)	Irr	−21.0	Prochaska et al. (2004)
060218	$7.54^{+0.16}_{-0.1}$ (integrated)	Irr	−15.9	Wiersema et al. (2007)
100316D	8.23 ± 0.15 (source A)	Spiral? Irr?	−18.8	This work

a dwarf spiral, in a small H II region right next to a very large star formation complex, whereas GRB 060218 and SN 2006aj occurred in a very faint, blue compact dwarf galaxy (Wiersema et al. 2007). This diversity is illustrated in Fig. 8.

Assuming that the properties of source A are at least roughly representative of the host galaxy as a whole, we can compare the spectroscopic properties with those of the other nearby GRB-SN hosts. Electron-temperature-based oxygen abundances have been derived for several of these (see Table 5). The case of GRB 980425 is of particular interest: besides many similarities between SN 1998bw and 2010bh, there are also several similarities in host galaxy properties. The T_e metallicities measured at the location of the GRB and at the location of a nearby, bright, WR star region (Hammer et al. 2006) are clearly similar to the metallicity measured for the H II region A in the host of GRB 100316D. In addition, the size and brightness (and possibly morphology) of these two hosts are comparable, though an important difference between the hosts of 980425 and 100316D is evident from Fig. 8: the morphology of the host of 100316D is highly disturbed, possibly indicative of a recent merger.

The host of GRB 980425 has been studied using integral field spectroscopy (Christensen et al. 2008), showing that the H II region in which the GRB exploded is similar in mass, SFR, reddening and line equivalent width to other H II regions in this host, with the exception of a bright WR-star rich H II region 800 pc away from the GRB site. In terms of metallicity, the WR region and GRB site have a somewhat lower metallicity than other H II regions in this host (Christensen et al. 2008). If this situation is comparable to the host of GRB 100316D, we may expect that the properties measured above of source A are indeed representative of most of the host galaxy properties.

8.3 Comparison to GRB 060218

In Section 8.1 we found that among the GRB-SNe, there is a clear commonality in the X-ray behaviour of 100316D and 060218. Comparing the prompt emission spectra in Section 5, we again find parallels in that both bursts seem to require a similar thermal component in addition to the typical GRB synchrotron emission for which the synchrotron peak is observed to move to lower energies with time. The time-evolving prompt spectral parameters are compared in Fig. 4. Both events have low isotropic equivalent energies, of the order of 4×10^{49} erg, and very little flux above 50 keV.

These two events lie in apparently quite different environments: 060218 in a faint, compact dwarf (Modjaz et al. 2006; Wiersema et al. 2007) and 100316D in a luminous, disturbed possibly spiral host galaxy. The metallicities are also different, with the host of 100316D likely being more metal-rich (though the metallicity is below solar). A prompt optical component, as observed in 060218, could not be detected in 100316D, but conditions for its detection

were far less optimal in this case due to the superposition on a brighter host galaxy and the possibility of a higher extinction along the line of sight. The higher intrinsic X-ray column density we measure for 100316D compared with similar modelling of 060218 does not necessarily imply a higher optical extinction (Watson et al. 2007; Campana et al. 2010).

In summary, both 100316D and its predecessor 060218 are nearby ($z = 0.059$, 0.033), long-duration ($T_{90} \geq 1300$, 2100 s), initially relatively constant in X-ray flux (Fig. 6), spectrally soft (very few or no counts above 100 keV; low $E_{\rm pk}$, Fig. 4), subenergetic (both have $E_{\rm iso} \sim 4 \times 10^{49}$ erg) GRBs with an associated SN. These two events show similar prompt emission properties and stand out among the GRB-SNe subsample considered here for their unusual X-ray evolution. However, their host galaxies are rather different in morphology and metallicity, with the host of 100316D more closely resembling the host of 980425.

The thermal X-ray component, with a luminosity, temperature and radius similar to that observed in 060218, dictates that the shock breakout of the SN must be considered. The optical/UV thermal component observed in 060218 is not seen here: if the extinction is similar we would expect a shock breakout similar to 060218 to be two or more times fainter in 100316D and with the relatively brighter host galaxy, it is perhaps no surprise that early optical emission is not detected with UVOT. The presence of a thermal component in the prompt γ-ray emission of Burst And Transient Source Experiment (BATSE) GRBs, in addition to non-thermal emission, was proposed by Ryde (2004). The discovery of thermal components in the *Swift* XRT X-ray spectra shown here for 100316D and in Campana et al. (2006) for 060218 will therefore be important to consider in future studies of GRB prompt emission. The dominant component of the high energy emission in 100316D remains the synchrotron-like non-thermal spectrum common to all types of GRB (with and without SNe) thought to originate in internal shocks in a relativistic jet. The long duration of the early X-ray emission is curious, and exceedingly rare, perhaps suggesting that a greater reservoir of material is available to feed the central engine and prolong its activity.

The discovery of GRB 100316D and its associated supernova SN 2010bh and the analyses of its high energy emission and host galaxy properties presented here illustrate the diversity in GRB-SNe characteristics that must be understood if we are to fully appreciate the relationship between GRBs and core-collapse SNe.

ACKNOWLEDGMENTS

This work made use of data supplied by the UK *Swift* Science Data Centre at the University of Leicester. This work is based on observations made with ESO Telescopes at the La Silla or Paranal Observatories under programme IDs 084.D-0939, 083.A-0644 and 084.A-0260(B). This work is also based on observations made with the NASA/ESA Hubble Space Telescope, obtained at the Space Telescope Science Institute, which is operated by the Association of Universities for Research in Astronomy, Inc., under NASA contract NAS 5-26555: these observations are associated with programme 11709. We thank STScI staff for their efforts in implementing the *HST* ToO observation, particularly Alison Vick. We acknowledge the wider *Swift* team for their many contributions. RLCS, KW, AR, JPO, KLP and PAE acknowledge financial support from STFC. Financial support of the British Council and Platform Beta Techniek through the Partnership Programme in Science (PPS WS 005) is gratefully acknowledged (KW). The Dark Cosmology Centre is funded by the Danish National Research Foundation. DNB acknowledges NASA contract NAS5-00136. AJvdH was supported by an appointment to the NASA Postdoctoral Program at the MSFC, administered by Oak Ridge Associated Universities through a contract with NASA.

REFERENCES

Alard C., 2000, A&AS, 144, 363
Amati L., 2006, MNRAS, 372, 233
Amati L., Della Valle M., Frontera F., Malesani D., Guidorzi C., Montanari E., Pian E., 2007, A&A, 463, 913
Arnaud K., 1996, in Jacoby J. H., Barnes J., eds, ASP Conf. Ser. Vol. 101, Astronomical Data Analysis Software and Systems V. Astron. Soc. Pac., San Francisco, p. 17
Asplund M. M., Grevesse N., Sauval A. J., Allende-Prieto C., Kiselman D., 2004, A&A, 417, 751
Band D. et al., 1993, ApJ, 413, 281
Barthelmy S. et al., 2005, Space Sci. Rev., 120, 143
Blustin A. J. et al., 2006, ApJ, 637, 901
Bufano F. et al., 2010, GCN Circular, 10543
Burrows D. N. et al., 2005, Space Sci. Rev., 120, 165
Campana S. et al., 2006, Nat, 442, 1008
Campana S., Thoene C. C., de Ugarte Postigo A., Tagliaferri G., Moretti A., Covino S., 2010, MNRAS, 402, 2429
Chapman R., Tanvir N. R., Priddey R. S., Levan A. J., 2007, MNRAS, 382, L21
Chornock R. et al., 2010, ApJ, submitted (arXiv:1004.2262)
Christensen L., Vreeswijk P. M., Sollerman J., Thöne C. C., L Floc'h E., Wiersema K., 2008, A&A, 490, 45
Cobb B. E., Bailyn C. D., van Dokkum P. G., Natarajan P., 2006, ApJ, 645, L113
Costa E. et al., 1997, Nat, 387, 783
De Pasquale M. et al., 2006, A&A, 455, 813
Della Valle M. et al., 2006, ApJ, 642, L103
D'Odorico S. et al., 2006, in McLean I. S., Masanori I., eds, Proc. SPIE Vol. 6269, Ground-based and Airborne Instrumentation for Astronomy. SPIE, Bellingham, p. 98
Evans P. A. et al., 2007, A&A, 469, 379
Evans P. A. et al., 2009, MNRAS, 397, 1177
Fan Y.-Z., Zhang B.-B., Xu D., Liang E.-W., Zhang B., 2010, ApJ, in press, preprint (arXiv:1004.5267)
Ferrero P. et al., 2006, A&A, 457, 857
Fruchter A. S. et al., 2006, Nat, 441, 463
Fynbo J. P. U. et al., 2006, Nat, 444, 1047
Fynbo J. P. U. et al., 2009, ApJS, 185, 526
Galama T. J. et al., 1998, Nat, 395, 670
Gal-Yam A. et al., 2006, Nat, 444, 1053
Gehrels N. et al., 2004, ApJ, 611, 1005
Gehrels N. et al., 2008, ApJ, 689, 1161
Ghisellini G., Ghirlanda G., Tavecchio F., 2007, MNRAS, 382, L77
Goldoni P. et al., 2006, in McLean I. S., Masanori I., eds, Proc. SPIE Vol. 6269, Ground-based and Airborne Instrumentation for Astronomy. SPIE, Bellingham, p. 80
Gonzalez Delgado R. M., Leitherer C., Heckman T. M., 1999, ApJS, 125, 489
Hammer F., Flores H., Schaerer D., Dessauges-Zavadsky M., Le Floc'h E., Puech M., 2006, A&A, 454, 103
Hjorth J. et al., 2003, Nat, 423, 847
Holland S. T. et al., 2010, ApJ, 717, 223
Hurkett C. P. et al., 2008, ApJ, 679, 587
Izotov Y. I., Thuan T. X., Lipovetsky V. A., 1994, ApJ, 435, 647
Jakobsson P. et al., 2006, A&A, 447, 897
Kalberla P. M. W., Burton W. B., Hartmann D., Arnal E. M., Bajaja E., Morras R., Poppel W. G. L., 2005, A&A, 440, 775
Kaneko Y. et al., 2007, ApJ, 654, 385
Kennicutt R. C., 1998, ARA&A, 36, 189
Kulkarni S. R. et al., 1998, Nat, 395, 663

Levan A. J., Tanvir N. R., D'Avanzo P., Vergani S. D., Malesani D., 2010, GCN Circular, 10523
Levesque E. M., Berger E., Kewley L. J., Bagley M. M., 2010, AJ, 139, 694
Liang E., Zhang B., Virgili F., Dai Z. G., 2007, ApJ, 662, 1111
Malesani D. et al., 2004, ApJ, 609, L5
Mazzali P. A. et al., 2005, Sci, 308, 1284
Mazzali P. A. et al., 2006, Nat, 442, 1018
Mirabal N., Halpern J. P., An D., Thorstensen J. R., Terndrup D. M., 2006, ApJ, 643, L99
Modjaz M. et al., 2006, ApJ, 645, L21
Oates S. R., De Pasquale M., Stamatikos M., 2010, GCN Circular, 10520
Osterbrock, 1989, Astrophysics of Gaseous Nebulae and Active Galactic Nuclei. Univ. Sci. Books, Mill Valley, CA
Paragi Z. et al., 2010, Nat, 463, 516
Pei Y. C., 1992, ApJ, 395, 130
Perley D. A., Foley R. J., Bloom J. S., Butler N. R., 2006, GCN Circular, 5387
Pian E., Antonelli L. A., Piro L., Feroci M., 1998, GCN Circular, 158
Pian E. et al., 2000, ApJ, 536, 778
Pian E. et al., 2006, Nat, 442, 1011
Piro L. et al., 2005, ApJ, 623, 314
Poole T. S. et al., 2008, MNRAS, 383, 627
Prochaska J. X. et al., 2004, ApJ, 611, 200
Rees M. J., Mészáros P., 1994, ApJ, 430, L93
Roming P. W. A. et al., 2005, Space Sci. Rev., 120, 95
Ryde F., 2004, ApJ, 614, 827
Sakamoto T. et al., 2008, ApJS, 175, 179
Sari R., Piran T., Narayan R., 1998, ApJ, 497, L17
Schlegel D. J., Finkbeiner D. P., Davis M., 1998, ApJ, 500, 525
Soderberg A. M. et al., 2006, Nat, 442, 1014
Soderberg A. M. et al., 2010, Nat, 463, 513
Sollerman J., Östlin G., Fynbo J. P. U., Hjorth J., Fruchter A., Pedersen K., 2005, New Astron., 11, 103
Sollerman J. et al., 2006, A&A, 454, 503
Stamatikos M. et al., 2010, GCN Circular, 10496
Stanek K. Z. et al., 2003, ApJ, 591, L17
Starling R. L. C. et al., 2008, MNRAS, 384, 504
Starling R. L. C., Evans P. A., Stamatikos M., 2010, GCN Circular, 10519
Stratta G., Perri M., Siegel M. H., Krimm H. A., Barthelmy S. D., Roming P., Burrows D. N., Gehrels N., 2009, GCN Report 212.1
Svensson K. M., Levan A. J., Tanvir N. R., Fruchter A. S., Strolger L. G., 2010, MNRAS, 405, 57
Tanvir N. R. et al., 2010, ApJ, in press (arXiv:0812.1217)
Toma K., Ioka K., Sakamoto T., Nakamura T., 2007, ApJ, 659, 1420
Vergani S., Levan A. J., D'Avanzo P., Covino S., Malesani D., Hjorth J., Tanvir N. R., Antonelli L. A., 2010, GCN Circular, 10513
Verner D. A., Ferland G. J., Korista K. T., Yakovlev D. G., 1996, ApJ, 465, 487
Watson D. et al., 2004, ApJ, 605, L101
Watson D., Hjorth J., Fynbo J. P. U., Jakobsson P., Foley S., Sollerman J., Wijers R. A. M. J., 2007, ApJ, 660, L101
Waxman E., Mészáros P., Campana S., 2007, ApJ, 667, 351
Wiersema K. et al., 2007, A&A, 464, 529
Wiersema K., D'Avanzo P., Levan A. J., Tanvir N. R., Malesani D., Covino S., 2010, GCN Circular, 10525
Willingale R. et al., 2004, MNRAS, 349, 41
Wilms J., Allen A., McCray R., 2000, ApJ, 542, 914
Woosley S. E., Bloom J. S., 2006, ARA&A, 44, 507
Zeh A., Klose S., Hartmann D. H., 2005, in Chen P. et al., eds, Proc. 22nd Texas Symp. on Relativistic Astrophysics. SLAC, Stanford, CA, p. 574, preprint (astro-ph/0503311)

This paper has been typeset from a TEX/LATEX file prepared by the author.

© 2010 The Authors, MNRAS **411,** 2792–2803
Monthly Notices of the Royal Astronomical Society © 2010 RAS